



Effects of Hurricane Irma on residual flows and saltwater intrusion in a subtropical estuary



Gisselle E. Guerra-Chanis^{a,c,*}, Sangdon So^b, Arnoldo Valle-Levinson^a

^a Department of Civil and Coastal Engineering, University of Florida, Gainesville, FL 32611, USA

^b Applied Technology and Management, Gainesville, FL, 32605, USA

^c Centro de Investigaciones Hidráulicas e Hidrotécnicas, Universidad Tecnológica de Panamá, Panamá

ARTICLE INFO

Article history:

Received 29 April 2020

Received in revised form 10 September 2020

Accepted 24 November 2020

Available online 25 November 2020

Keywords:

Saltwater intrusion

Freshwater pulse

Hurricane Irma

Salt fluxes

Salt-wedge estuary

ABSTRACT

The variability of residual flows and saltwater intrusion was evaluated for the duration of a hurricane-related freshwater pulse in a subtropical estuary, the Suwannee River. Increased rainfall affected the river's watershed when Hurricane Irma skirted the west coast of Florida in September 2017. The river remained short of reaching flood stages, but the increased river discharge was enough to modify the residual circulation and restrict saltwater intrusion. Current velocity profiles and hydrographic variables were collected in five tidal-cycle experiments to study the lower estuary's response to the peak river discharge and its subsequent relaxation. Data were recorded in three cross-estuary transects. In addition, continuous salinity measurements were recorded for 48 days over the shallow portion of the seaward transect. Results showed that the subtidal water-level slope inside the estuary, between the mouth and a river station at Wilcox, modified the residual circulation and restricted the intrusion of salt water. During high tide, salt water entered the estuary due to tidal pumping even though residual circulation was seaward in the cross-section. Residual seaward flows persisted for the duration of the hurricane-related freshwater pulse. After relaxation of the freshwater pulse, saltwater intrusion was observed in the time series over the shallow portion. This saltwater intrusion responded to changes in wind forcing, with largest intrusions when the wind blew into the estuary, i.e., toward the N and NW.

© 2020 Elsevier B.V. All rights reserved.

1. Introduction

Estuaries are vulnerable to sea level rise and flooding due to extreme weather events. Hurricanes and tropical storms are usually accompanied by intense rainfall (>30 mm/day) that can increase river discharge and upstream water (Smith et al., 2010; Villarini et al., 2011). Increased river discharge and water-level slopes from head to mouth of an estuary can modify its residual circulation and hence modify the length of saltwater intrusion. Differences in water level between the head and the mouth of the estuary are attributed to bathymetric features, river stage, astronomical tides and atmospheric forcing. Estuarine residual circulation, i.e., the exchange between salt water and fresh water in estuaries, and the limit of saltwater intrusion depend on the time scale of the above-mentioned (Geyer and MacCready, 2014; Cho et al., 2012; Valle-Levinson et al., 2002; MacCready, 2007) and the response time of the estuary (MacCready, 2007; Warner et al., 2005). Extreme freshwater pulses of similar duration to

the response time of the estuary can modify the residual circulation and the length of saltwater intrusion (Valle-Levinson, 2012; MacCready, 1999).

Estuaries can respond to a freshwater pulse in two ways: by having unidirectional outflows in a cross-section, or by intensifying the bi-directional exchange flow (MacCready, 2007; Valle-Levinson, 2012). The Delaware estuary, a weakly stratified estuary with a mean depth of ~15 m, presented unidirectional outflows after a pulse of freshwater. Subtidal outflows developed 8–20 days after a change in river discharge at the estuary's mouth (Garvine, 1991). A similar estuarine response was observed in the Chesapeake Bay, following an extreme freshwater pulse (Valle-Levinson et al., 2002; Cho et al., 2012). After the passage of Hurricane Floyd, seaward subtidal velocities of 0.8 m/s were observed in the entire cross-section and salinity values decreased from 28 to 20 g/kg over 24 h (Valle-Levinson et al., 2002). The estuary recovered its pre-storm conditions after ~10 days (Valle-Levinson et al., 2002; Cho et al., 2012). Freshwater-related seaward flows in both Delaware Bay and Chesapeake Bay were intensified by the storm-related wind stress (Garvine, 1991; Valle-Levinson et al., 2002; Cho et al., 2012).

Freshwater pulses can therefore modify the magnitude and vertical structure of subtidal flows, and the transport of salt and

* Corresponding author at: Centro de Investigaciones Hidráulicas e Hidrotécnicas, Universidad Tecnológica de Panamá, Panamá.

E-mail address: gisselle.guerra@utp.ac.pa (G.E. Guerra-Chanis).

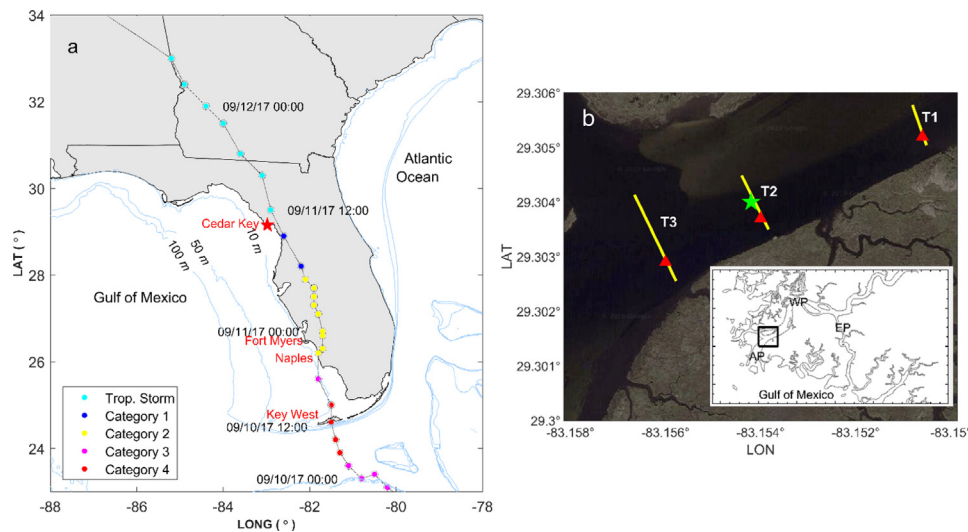


Fig. 1. Study area. (a) Track of Hurricane Irma, September 2017, where the red star shows the location of the Suwannee River estuary; (b) Location of the transects at the Suwannee River estuary. T1 is located upstream of T2 and T3. CTD stations along the transects are marked with red triangles and the green star represents the location of the moored CT (CT mouth). WP: West pass; AP: Alligator pass; EP: East pass. (For interpretation of the references to color in this figure legend, the reader is referred to the web version of this article.)

waterborne materials. The long-term transport and excursion of salt is linked to the residual circulation (Wu et al., 2010) and external forcings such as tides, river discharge and wind (Bowen and Geyer, 2003). The length of saltwater intrusion under different scenarios of river discharge was evaluated in the Tanshui River estuary, Taiwan, using numerical simulations (Wen-Cheng et al., 2001). In that study, salinity values at the mouth of the estuary decreased to zero after a 2-day pulse of freshwater. The system recovered to its previous stage after 5 days, when salinity increased to ~ 22 g/kg (Wen-Cheng et al., 2001).

The opposite behavior was documented in Wadley Pass of the Suwannee River estuary, a salt-wedge estuary located in the subtropical region of Florida. After a record flooding of $1100 \text{ m}^3/\text{s}$, a two-layer estuarine circulation was observed in the channel of a cross-section and it remained for ~ 20 days following the pulse of freshwater. After this time, net flows were weaker and seaward in the entire cross-section. Salinity measurements were not available, but it was hypothesized that the length of saltwater intrusion increased for the first ~ 20 days after the pulse of freshwater (Valle-Levinson, 2012).

This study evaluates the variability of residual flows and salinity during and after a hurricane-related freshwater pulse in a subtropical estuary. The Suwannee River was affected by increased rainfall after Hurricane Irma fringed the west coast of Florida in September 2017. The river remained short of reaching flood stages, with maximum values of $500 \text{ m}^3/\text{s}$. The increased river discharge was enough to modify the residual circulation at the mouth of the estuary and restrict saltwater intrusion. Contrary to what (Valle-Levinson, 2012) observed over a different branch of the Suwannee River delta (West Pass), here the hurricane-related freshwater pulse caused seaward flows in the entire water column. Five tidal-cycle experiments took place under different conditions of river discharge, wind forcing and spring-neap variability during an 8-week span after the hurricane. Continuous salinity measurements over a shoal of a lower estuary cross-section revealed wind-driven salinity pulses as the freshwater pulse was relaxing. The tidal-cycle experiments and the salinity measurements were close to the mouth of a delta branch with no previous knowledge of saltwater intrusion and residual flows. This study finds a contrasting response to that observed over a different branch of the delta, the Alligator Pass.

2. Study area

The Suwannee River originates at the Okefenokee Swamp in southeastern Georgia and flows southward and southwestward through Florida into the Gulf of Mexico. It is 392 km long and considered the second largest river system in Florida by its annual mean discharge of $288 \text{ m}^3/\text{s}$ and its drainage area of $25,770 \text{ m}^2$ (Valle-Levinson, 2012; Light et al., 2002). The Suwannee River estuary comprises the last 16 km of the river just before draining into the Gulf of Mexico (Fig. 1). The lower estuarine portion bifurcates into West Pass and East Pass, and West Pass in turn trifurcates into Northern, Wadley and Alligator Pass, in the middle of the entire delta (Laurel-Castillo and Valle-Levinson, 2020). The estuarine portion is mainly dominated by the influence of semidiurnal tides with an amplitude of 40–60 cm in spring tides and 20–35 cm during neap tides. Records from the USGS station at Wilcox indicate that tides can reach ~ 45 km upstream (Tillis, 1999). Winds with stresses >0.05 Pa affect the region during winter and fall with a dominant direction from NW and NE. Winds are weaker and more variable during spring with stresses <0.01 Pa. During summer, the predominant direction from S and SW, except during storm events (Valle-Levinson, 2012). This study focuses on Alligator Pass, one of the two branches of West Pass (Fig. 1), which has a mean depth of 2.2 m below Mean Sea Level and a width of 250–400 m. The study area presents a complicated bathymetry with scouring pits of 5–6 m, meandering channels and seagrass beds at its ocean limit (Valle-Levinson, 2012; Laurel-Castillo and Valle-Levinson, 2020) (see Fig. 1).

In September 2017, Hurricane Irma affected the Florida peninsula with heavy rainfall (>500 mm) and strong winds (>200 km/h or ~ 55 m/s). Before its landfall in the Florida Keys as a category 4 hurricane, Irma smashed the northern Caribbean Islands and northern Cuba as a category 5. The final landfall of Hurricane Irma was near Marco Island, Florida at 19:30 GMT on September 10, 2017 as a category 3 with maximum sustained winds of 185 km/h (Cangialosi et al., 2017). Irma continued to weaken after passing east of Tampa, Florida, and was downgraded to category 1 on September 11 (Fig. 1). Hurricane Irma weakened to a tropical storm at 12:00 on September 11, when it arrived at Cedar Key, Florida. Rainfall associated with the passage of Irma was between 254 and 381 mm across Florida and the Florida Keys (Cangialosi et al., 2017). For the period from 1961 to 1990, cumulative rainfall

means for September are usually between 25 and 76 mm for the Suwannee River (Tillis, 1999). During September 2017, the USGS station at Wilcox in the Suwannee River recorded a total rainfall of 213 mm with a peak value of 87 mm on September 11, 2017. This means that the one-day rainfall attributed to Irma was 41% of the total rainfall recorded in September 2017. Storm surge due to Hurricane Irma had a marked difference between east and west coasts (So et al., 2019). On the west coast a maximum surge of 1.6 m was recorded at Naples and a negative storm surge of -2.7 m at Cedar Key. On the east coast a maximum surge of 2.4 m was recorded at Fernandina Beach. This marked difference of storm surge at the Florida peninsula was attributed to the wind divergence during the passage of the storm (So et al., 2019).

The direct passage of Tropical Storm Irma over the watershed of the Suwannee River presented the opportunity to study the response of a subtropical estuary during and after a freshwater pulse. This response will be described by salinity variations at different depths and by the variability of the residual flows. The spatial structure of the residual flows is described during and after the freshwater pulse for spring and neap tides. This study also addresses salinity variability for a period of 48 days and explores the dynamics associated with the hurricane-related freshwater pulse.

3. Methodology

Vessel-based tidal-cycle surveys of flow and salinity were combined with moored salinity time series to understand the variability of saltwater intrusion and residual flows due to a storm-related freshwater pulse. Ancillary data, consisting of river discharge, wind and tides were used to explain the freshwater pulse effect on the estuarine hydrodynamics and relate it to main forcings. The following subsections explain how the data were collected for further analysis.

3.1. Data collection

Current velocity and hydrographic profiles were sampled at Alligator Pass, in the lower Suwannee River delta, throughout five tidal-cycle surveys from September to November 2017. Each survey covered three cross-estuary transects after the influence of Hurricane Irma. Starting upstream, the transects were named T1, T2 and T3, with T3 located 2 km upstream from the mouth of the entrance to Alligator Pass (Fig. 1). The distance between transects was ~ 300 m, covering an approximate surface area of $90,000$ m². Transect 3 (T3) was 200 m while transects 1 and 2 (T1 & T2) were 100 m; with the deepest channel of ~ 6 m at T2. The five tidal-cycle experiments captured different portions of the spring-neap cycle variability. Due to diurnal inequalities, these experiments captured different flood-ebb asymmetries. The specific dates of the tidal-cycle experiments are detailed in Table 1. Transects were located at the main channel of Alligator Pass in the Suwannee River delta. The distance between transects was ~ 300 m so that the salt wedge was easily identified in at least one of the transects.

Current velocities were collected with a 1200 kHz Teledyne RD Instruments Acoustic Doppler Current Profiler (ADCP). A SonTek CastAway conductivity-temperature-depth (CTD) recorder was used to sample hydrographic profiles at a frequency of 5 Hz. Profiles were only obtained in the deepest point of each transect, ~ 4 – 6 m deep, to observe expected maximum stratification (e.g. Fischer, 1972; Valle-Levinson and Lwiza, 1997). The downward-pointing ADCP was mounted on a small catamaran and towed from the port side of a boat. The boat navigated at idle speed (~ 1.5 m/s) to ensure current velocity spatial coverage. Each transect was repeated between 15 and 22 times for ~ 13 h

to capture the intratidal flow variability and the density field for one semidiurnal tidal cycle. Due to navigation constraints, the transects did not cover the entire breadth of the estuary.

In addition, near-bottom salinity and temperature were recorded at the entrance to Alligator Pass from September 16 to November 02, 2017, a total of 48 days. A Sea-Bird SBE 37 conductivity-temperature-depth recorder (CTD) was moored at a fixed point in T2 at a depth of ~ 2 m (Fig. 1). This mooring will be referred to as “CT mouth” to distinguish it from the CTD casts at the transects. The CT mouth had a sampling interval of five minutes. Ancillary data were retrieved for the same period to explain saltwater variability on the basis of different forcings. River discharge and water level time series were obtained from the USGS (US Geological Survey) station at Wilcox 023323500 ($29^{\circ}35'22''$ N, $82^{\circ}56'12''$ W), located ~ 43 km upstream from the Suwannee River's mouth. River discharge values were obtained every 15 min, available from the US Geological Survey site (<https://waterdata.usgs.gov/nwis>). Hourly wind data were obtained from meteorological station #CDRF1 at Cedar Key, FL, located ~ 23 km to the southwest of the river's mouth. Wind data are available through the NOAA website (http://www.ndbc.noaa.gov/station_history.php?station=cdrf1).

3.2. Data processing

Velocity profiles from the towed ADCP were recorded every 0.3 s and then averaged over five profiles to get a horizontal resolution of ~ 2 m. The vertical bin size of each velocity measurement was 25 cm and the first current measurement was 40 cm from the surface. Underway velocity measurements were trimmed to remove: (i) profiles collected while traveling from one transect to the other (along estuary tracks), (ii) data influenced by side-lobe effects, and (iii) values that exceeded 10 cm/s in the absolute error velocity (Muste et al., 2004). Compass calibration and boat velocity corrections were effected on the ADCP current velocities by following the method of Joyce (1989) and Pollard and Read (1989). After correcting the current velocity profiles, they were organized in a regular matrix of north and east components for each transect repetition. A semidiurnal band (D_2) of 12.42 h, and a residual flow were fitted, via least-squares, to the current velocity time series at each point of the regular matrix. This process was followed for the three transects and for each survey. The least-squares fit has the form:

$$[u, v] = [u_0, v_0] + [u_{D_2}, v_{D_2}] \sin(\omega_{D_2} t - [\theta_{uD_2}, \theta_{vD_2}]) \quad (1)$$

where u, v are the observed velocity components in the east and north directions, respectively; u_0, v_0 are residual velocities at each regular matrix point. The amplitude for the semidiurnal band (D_2) is represented with u_{D_2}, v_{D_2} ; ω_{D_2} is the semidiurnal angular frequency; t is time in days and $\theta_{uD_2}, \theta_{vD_2}$ are the phases relative to the beginning of the observations (Valle-Levinson et al., 2015; So et al., 2020). The three parameters for each velocity component obtained from each fit are, say for the east component: u_0, u_{D_2} , and θ_{uD_2} .

Also in the tidal-cycle experiments, hydrographic profiles were obtained every half an hour to an hour over the deepest portion of each transect to capture vertical stratification (Fig. 3). Absolute salinity (g/kg) was estimated with the Thermodynamic Equation of Seawater – TEOS 2010. This estimation relates the conductivity, temperature and pressure data sampled with the CTD to the salinity in g/kg (McDougall and Barker, 2011; McDougall et al., 2012). Vertical profiles of salinity were arranged in contour diagrams of time vs depth, also known as Hovmöller or phase diagrams. Tidally averaged salinity profiles were then calculated for each transect.

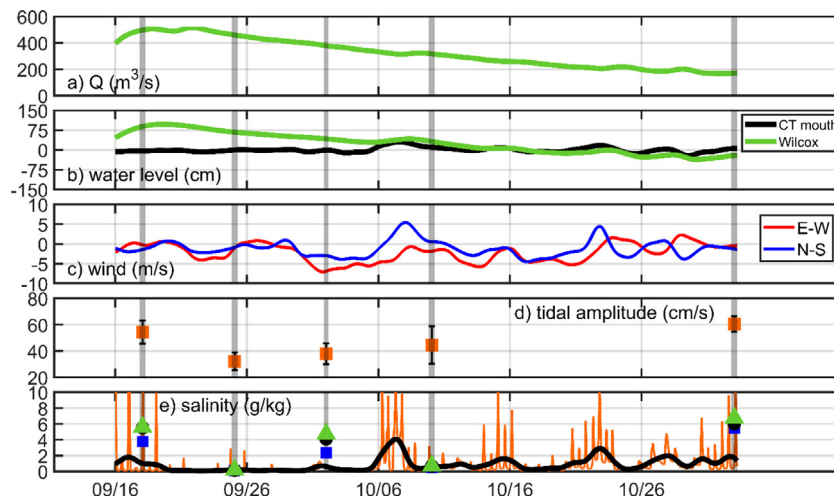


Fig. 2. Time series from September 16 to November 02, 2017 of climate forcings. (a) river discharge (m^3/s) at Wilcox USGS station; (b) water level (cm) at Wilcox USGS station (green) and at the river's mouth (black); (c) wind velocity (m/s) components the N-S (blue) and E-W (red) component, following the oceanographic convention; (d) mean tidal amplitude velocities (cm/s) from the ADCP measurements; (e) subtidal (black) and tidal (orange) salinity at the river's mouth in g/kg. Symbols in (e) indicate vertically and tidally averaged salinities at each transect, T1 (blue square), T2 (black circle), T3 (green triangle). Time series were smoothed with a Lanczos filter centered at 30 h. Dates of tidal-cycle experiments are marked with gray vertical bands. (For interpretation of the references to color in this figure legend, the reader is referred to the web version of this article.)

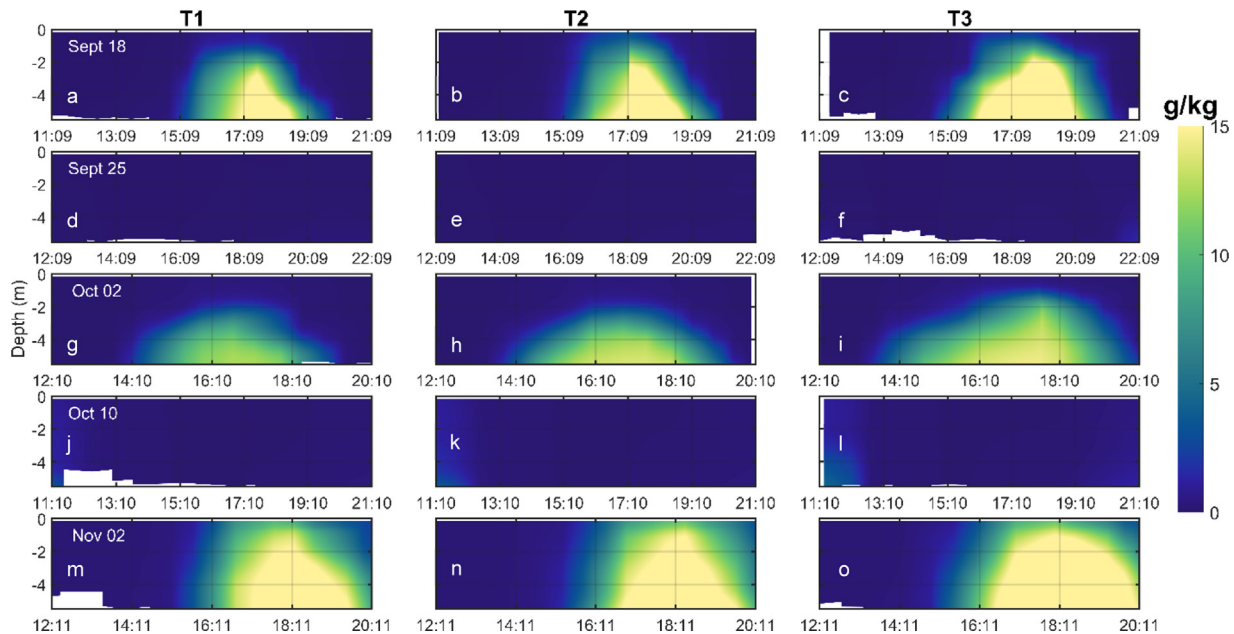


Fig. 3. Time series of salinity from the tidal-cycle experiments. From left to right, T1, T2, and T3, and from top to bottom, the date of the experiments: September 16, September 25, October 2, October 10 and November 2 of 2017. For each panel the y-axis indicates depth (m) and the x-axis indicates the time of the survey.

Table 1
Tidal-cycle experiments of current velocities and salinities.

Tidal-cycle experiment	Date (2017)	Tidal range (m)	Spring/Neap tides	Mean residual amplitudes (cm/s)	Mean salinity (g/kg)
Sept18	September 18	1.14–0.03	1 day after spring	53	4.97
Sept25	September 25	1.01–0.15	3 days before neap	32	0.16
Oct02	October 02	1.01–0.13	3 days before spring	38	3.73
Oct10	October 10	1.09–0.00	2 days before neap	45	0.62
Nov02	November 02	1.00–0.10	2 days before spring	61	6.09

For the moored CT (*CT mouth*), intratidal variations were removed from the salinity and water level time series with a low-pass Lanczos filter centered at 30 h. Water level and river discharge were obtained at Wilcox USGS station. To calculate water level slopes, these variables were first demeaned and then

filtered also with a low-pass Lanczos filter centered at 30 hours (Payandeh et al., 2019; Salas-Monreal and Valle-Levinson, 2008; Henrie and Valle-Levinson, 2014). Wind speeds and directions from the Cedar Key NOAA station were decomposed in east and north components following the oceanographic convention,

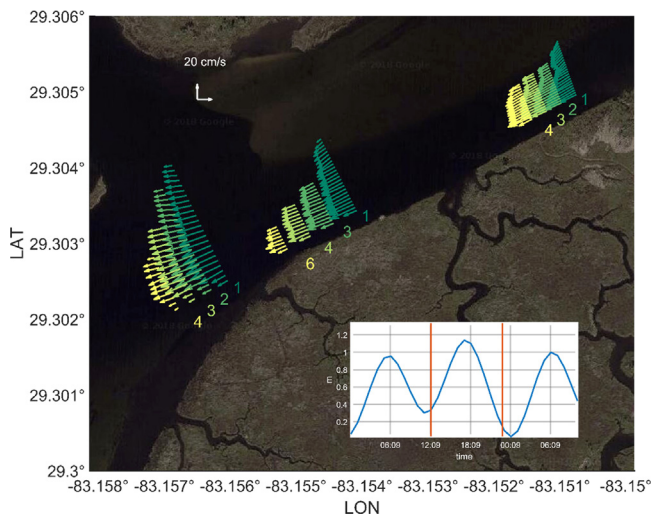


Fig. 4. Cross-section residual circulation and tide predictions for September 18, 2017. Green color vectors for close to surface velocities and yellow color vectors for close to the bottom velocities. Numbers indicate water depth (m) from the surface. Tide predictions (m) from Cedar Key, FL with orange vertical lines indicating the duration of the experiment. (For interpretation of the references to color in this figure legend, the reader is referred to the web version of this article.)

which reports winds in the direction toward which they blow. The wind components were also smoothed with the 30-h low-pass Lanczos filter. Tide predictions were obtained from the Cedar Key Station CDRF1.

4. Results

Observations were carried out under different conditions of river discharge, wind forcing and spring-neap cycle. This section presents the main features of the residual and tidal flows, and the vertical structure of salinity in the five tidal-cycle experiments. Residual flows were fluvially dominated during the freshwater pulse. Salinity mainly enters the estuary during flood tidal phases and with the main channel. Lowest records of salinities occurred during the ebb phase of the tide and just before neap tides. The Results section ends with time series of salinity near the mouth of the estuary and its corresponding forcings (river discharge, wind, river stage and tides). Northward wind increased the length of saltwater intrusion after the peak of freshwater in Wilcox.

4.1. Residual flows

River discharge peaked twice at Wilcox station after Hurricane Irma: on September 19 with $505 \text{ m}^3/\text{s}$, and on September 22 (3 days later) with $517 \text{ m}^3/\text{s}$ (Fig. 2a). The tidal-cycle experiment of September 18 (Sept 18) took place before the two peaks of river discharge at Wilcox, when the river discharge was close to $500 \text{ m}^3/\text{s}$. Residual flows were obtained from least-squares fits (Eq. (1)) at each point of a regular grid of velocity data along each transect. From mid-September to the beginning of November 2017, these residual flows were unidirectional (Figs. 4–8). Ebb-tide and flood-tide durations were not equal at each tidal-cycle experiment. In the first tidal-cycle experiment, data collection coincided with spring tides (Fig. 2d). Ebb-tide duration was longer than the flood tide (inset of Fig. 4). The strongest residual outflows were located near the surface and decreased with depth. Salinity variations were depth-dependent in the three transects. Highest salinity values of 20 g/kg appeared close to the peak of flood tide and became zero before and after the

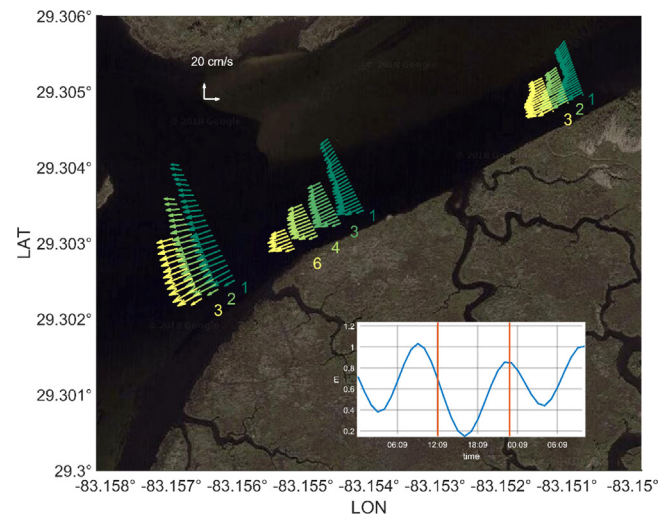


Fig. 5. Cross-section residual circulation and tide predictions for September 25, 2017. Green color vectors for close to surface velocities and yellow color vectors for close to the bottom velocities. Numbers indicate water depth (m) from the surface. Tide predictions (m) from Cedar Key, FL with orange vertical lines indicating the duration of the experiment. (For interpretation of the references to color in this figure legend, the reader is referred to the web version of this article.)

flood peak. Water column was stratified during high tide (17:09–18:09 GMT) related to saltwater intrusion in $\sim 65\%$ of the water column, without reaching the surface. Saltiest waters (by more than 4 g/kg) remained in the most seaward transect (T3) and decreased upstream (Fig. 3a–c). The hurricane-related freshwater pulse could have prevented the water column from being well mixed during the flood phase of spring tides. It is also possible that this is the regular behavior in Alligator pass, i.e. a salt-wedge system during tidal flood. In partially stratified or even strongly stratified systems, increased vertical mixing is expected by the end of flood during spring tides (Simpson et al., 1990; Friedrichs and Aubrey, 1988). However, isolated CTD profiles in Alligator Pass at other times of the year have suggested salt wedge development during flood tides. Wind direction was southerly in this experiment with weak speeds of $< 1 \text{ m/s}$ (Fig. 2c).

The tidal-cycle experiments of September 25 (Sept 25) and October 10 (Oct 10) took place in the transition to neap tides (Fig. 5), and the tidal-cycle experiment of October 02 (Oct 02) during the transition to spring tides (~ 3 days before spring tides). The strongest residual outflows were observed in the tidal-cycle experiment of October 10 (Oct 10), during the transition to neap tides (Fig. 7). Freshwater occupied the entire water column, i.e., no saltwater intrusion, during Sept 25 and Oct 10. Salinity increased weakly from 0.2 to 1 g/kg in the tidal-cycle experiment of Oct 10 (Fig. 3). Low-pass filtered winds were $\sim 1 \text{ m/s}$, blowing toward the SW on September 25 and toward the NW on Oct 10 (Fig. 2c).

During Oct 02 the freshwater pulse was receding at Wilcox station, changing from $450 \text{ m}^3/\text{s}$ to $300 \text{ m}^3/\text{s}$ (Fig. 2a). Therefore, freshwater occupied the entire water column until 17:10 GMT when high tide brought saltier water into the estuary. During high tide, the water column became stratified with a vertical surface-to-bottom contrast of 15 g/kg . The surface layer of freshwater thinned seaward, from T1 to T3. Around 19:10 GMT just after the high tide, freshwater reoccupied the entire water column (Fig. 3 g–i). Flood tide was shorter than ebb tide (inset Fig. 6) and salty water was observed close to the bottom in the three transects (Fig. 3 g–i). This stratification must have been enhanced by down-estuary winds (Fig. 2c), which can enhance vertical stratification (Scully et al., 2009, 2005).

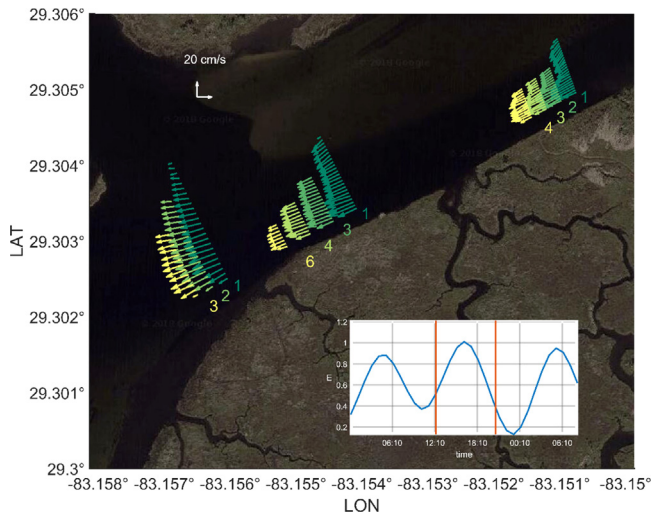


Fig. 6. Cross-section residual circulation and tide predictions for October 02, 2017. Green color vectors for close to surface velocities and yellow color vectors for close to the bottom velocities. Numbers indicate water depth (m) from the surface. Tide predictions (m) from Cedar Key, FL with orange vertical lines indicating the duration of the experiment. (For interpretation of the references to color in this figure legend, the reader is referred to the web version of this article.)

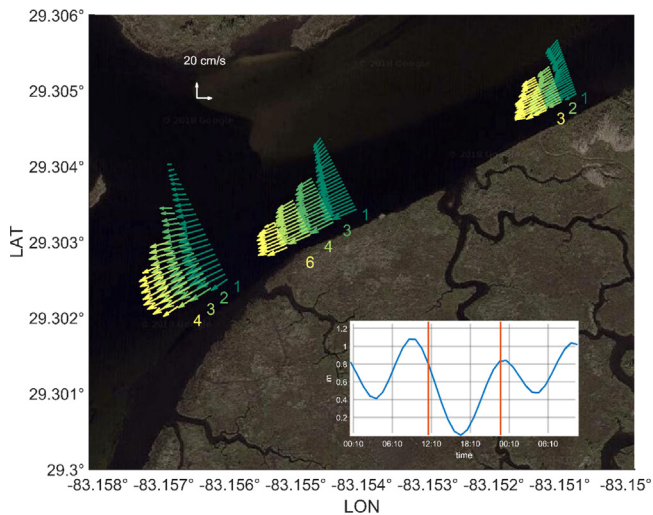


Fig. 7. Cross-section residual circulation and tide predictions for October 10, 2017. Green color vectors for close to surface velocities and yellow color vectors for close to the bottom velocities. Numbers indicate water depth (m) from the surface. Tide predictions (m) from Cedar Key, FL with orange vertical lines indicating the duration of the experiment. (For interpretation of the references to color in this figure legend, the reader is referred to the web version of this article.)

The last tidal-cycle experiment of November 02 (Nov 02) coincided with a river discharge of $200 \text{ m}^3/\text{s}$, and two days before spring tides. At this point, values of river discharge at Wilcox returned to pre-hurricane conditions, ~ 45 days later (Fig. 2a). For the first time, subtidal water levels at the river mouth were higher ($>20 \text{ cm}$) than subtidal water levels at Wilcox (Fig. 2b). Within the first four hours of the tidal-cycle experiment, only freshwater was present in the water column. Then, salinities increased rapidly close to high tide. The temporal change in salinity was centered at 16:11 GMT, when salinities increased from 0 to 15 g/kg in one hour (Fig. 3 m–o). This tidal intrusion front appeared first at T3 & T2 and 20 min later was observed at T1

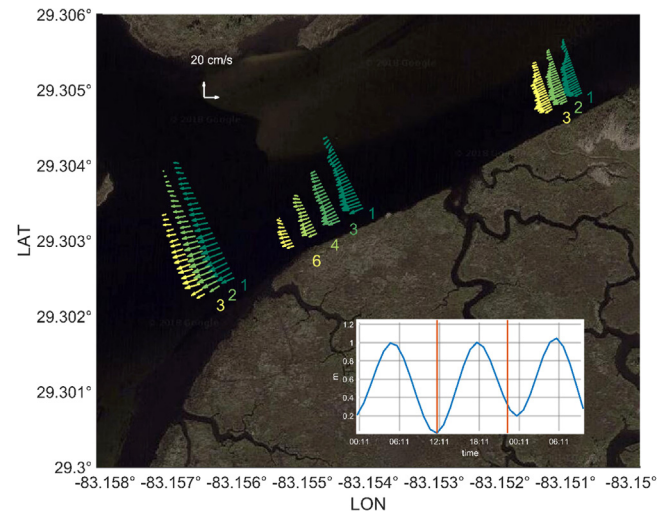


Fig. 8. Cross-section residual circulation and tide predictions for November 02, 2017. Green color vectors for close to surface velocities and yellow color vectors for close to the bottom velocities. Numbers indicate water depth (m) from the surface. Tide predictions (m) from Cedar Key, FL with orange vertical lines indicating the duration of the experiment. (For interpretation of the references to color in this figure legend, the reader is referred to the web version of this article.)

(upstream). Maximum salinities in the three transects were located closer to the bottom and tidally averaged salinities showed a stably stratified water column (Fig. 3 m–o). Flood to ebb tidal asymmetries were less marked than in previous tidal-cycle experiments (inset of Fig. 8). Residual flows were still directed seaward, with strongest flows in the channel and weakest outflows over the shoals in the three transects (Fig. 8). This flow structure was consistent with open channel flows.

4.2. Saltwater intrusion

After September 11, 2017, river discharge and water levels increased at Wilcox (upstream in the river) due to rainfall on the Suwannee River watershed. Water level peaked rapidly at a rate of $\sim 0.22 \text{ m/day}$ and receded at a slower rate of 0.04 m/day (Fig. 2b). Flood stages were not reached by the influence of Hurricane Irma, but the river discharge was almost twice the annual mean of $288 \text{ m}^3/\text{s}$ (Light et al., 2002), and the amount of rainfall in a period of 24 h accounted for 41% of the monthly mean. From September 16th to October 7th, subtidal water levels at this upstream station at Wilcox were higher than subtidal water levels at the river mouth, while river discharge was $>300 \text{ m}^3/\text{s}$. By October 16th, the freshwater pulse relaxed and the subtidal water level slopes reversed sign, with higher levels at the estuary mouth and lower levels at Wilcox (Fig. 2b).

Positive slopes between the estuary mouth and Wilcox (subtidal water level increasing landward) occurred from September 16th to October 16th, 2017, with minimum positive slopes from Oct 6th to 16th (Fig. 2b). Negative slopes, albeit rather weak compared to before Oct 16th, appeared after the freshwater pulse receded, from Oct 17th to Nov 02 (\sim last 16 days of the deployment). After Oct 17th, salinity was recorded at the entrance to the estuary at depths ($<2 \text{ m}$), i.e., shallower than the salinities recorded within the transects (Fig. 1). Therefore, this record must have under-represented maximum salinity values intruding in the channel during such period.

Variations of wind direction and surface slope modified the saltwater intrusion at this location. Wind direction was predominantly toward the SW, but during several instances, saltwater

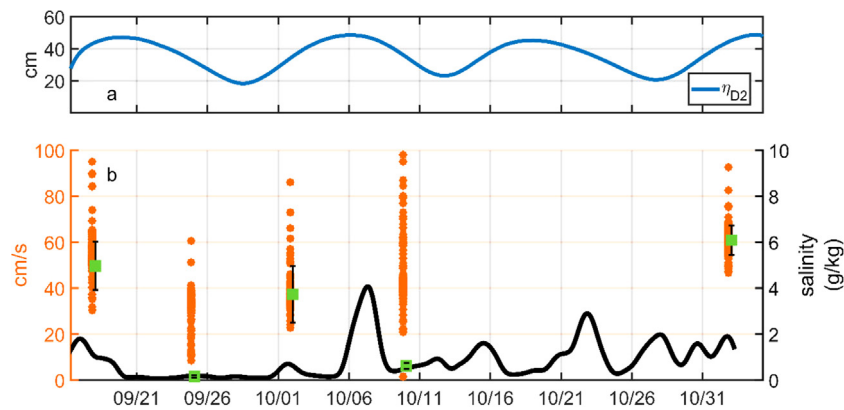


Fig. 9. Spring–neap cycle variability in tidal velocities and salinities. (a) amplitude of the semidiurnal band with tide predictions from Cedar Key, FL; (b) amplitude of tidal velocities in orange (cm/s) and salinity from the CT mouth (black line) and averaged salinities from the transects (green squares). Average salinities from the transects are in green squares with the standard deviation in black. (For interpretation of the references to color in this figure legend, the reader is referred to the web version of this article.)

intruded into the estuary when wind shifted toward the N, NW or NE (Fig. 2c). Four events of saltwater intrusion can be attributed to negative and minimum positive surface slopes responding to wind forcing. The largest intrusion occurred on October 6–7th, when a near-zero slope occurred between the mouth and Wilcox at the same time of low-pass filtered northward winds (>5 m/s). Subtidal salinity values at the mouth were 4 g/kg and persisted for 48 h. The peak of the second pulse of saltwater was centered on October 23rd when low-pass filtered winds were also northward at ~ 5 m/s. This suggested that once the freshwater pulse relaxed, wind forcing was playing the dominant role in subtidal saltwater intrusion. The third and fourth pulses of saltwater intrusion had subtidal values of 2 g/kg and coincided with weak low-pass filtered winds (1–2 m/s) toward the SW (Oct 16th) and NW (Oct 28th), respectively. As salinity measurements began while the river was still cresting, the pulse of saltwater on September 17th was the estuarine response to increased amplitude of tidal velocities, associated with spring tides (Fig. 9). Tidally and depth-sectional averaged salinities from transects also followed the spring–neap cycle variability. Maximum intrusion occurred at spring tides (experiments of Sep 18, Oct 10 and Nov 02) because of tidal advection (or tidal pumping), except for the survey of Sep 25 when there was no saltwater intrusion. The decrease in tidal current amplitudes and no saltwater intrusion on Sep 25 occurred just after the peak of freshwater pulse (Fig. 9).

The dynamics associated with the subtidal variability of water level during the freshwater pulse will be explained in the Discussion. Subtidal variations will be assessed through the balance among barotropic pressure gradient, frictional effects, and local accelerations. Salinity variations will be explained in terms of the mechanisms driving salt fluxes.

5. Discussion

The subtidal intrusion of saltwater into the estuary responded to the subtidal water level variability along the estuary and wind forcing. No saltwater intrusion occurred while the along-estuary water-level slope was at its largest. Once the freshwater pulse relaxed (after October 6th), saltwater entered the estuary (Fig. 2). During the river pulse, water level slope drove unidirectional seaward flows. This was different to the freshwater pulse of ~ 1000 m³/s in April 2009 when it was proposed that density gradients in Wadley Pass, west of Alligator Pass, caused exchange or bidirectional flows for the first 20 days while the river discharge was maximum (Valle-Levinson, 2012). The magnitude of the freshwater pulse, but most likely the distinct geometries of

the two delta branches might be responsible for the different estuarine response in the Suwannee River delta. This shall be the focus of future studies with numerical simulations.

The intrusion of saltwater at the mouth of Alligator Pass occurred at the same time as increased onshore wind events. The combined effects of two forcing mechanisms can explain the subtidal variations of water level at the mouth. The first one is the barotropic pressure gradient, $g \partial \eta / \partial x$, where $\partial \eta$ is the difference of subtidal water levels between the river (Wilcox station) and the estuary's mouth, and x is the along-estuary direction, positive landward. In other words, $\partial \eta / \partial x$ is the subtidal water level slope in the estuary. The second forcing is from the stress at the surface and the bottom. Thus, the depth-averaged subtidal momentum balance, assuming negligible baroclinic pressure gradients as suggested from the surveys, can be written as:

$$\frac{1}{A} \frac{\partial Q}{\partial t} = -g \frac{\partial \eta}{\partial x} + \left(\frac{\tau_s - \tau_b}{\rho H} \right) \quad (2)$$

where the left-hand side term is the local acceleration represented by the river discharge Q and the river's cross-sectional area A . The first term on the right-hand side is the barotropic pressure gradient along the estuary, where g is gravity acceleration, and the last term is the along-estuary frictional effects represented by surface τ_s and bottom τ_b stresses, in which ρ is water density and H is mean water depth. Local accelerations were first considered in the dynamics because of the “rapid” jump in river discharge. However, after scaling this term with typical values $A = 1300$ m², $dQ = 0.05$ m³/s and $dt = 900$ s, local accelerations were of order 10^{-8} m/s², three orders of magnitude smaller than the barotropic pressure gradient (10^{-5} m/s²). The local accelerations term was disregarded also because variations in river discharge were longer than the response time of the system.

The two terms that most likely governed the dynamics are underlined in Eq. (2), barotropic pressure gradient and friction. After removing the local accelerations, the subtidal momentum balance can be simplified as:

$$\frac{\partial \eta}{\partial x} = \frac{\tau_s - \tau_b}{g \rho H} \quad (3)$$

where bottom stress is $\tau_b = \rho C_b U^2$ [C_b is the dimensionless bottom drag coefficient with a canonical value of 0.0025 and U is the depth-averaged flow], surface or wind stress is $\tau_s = \rho_{air} C_d W^2$ [ρ_{air} is the density of air (1.225 kg/m³), C_d is the drag coefficient between air and water interface and W is the along-estuary wind speed]. Following the approximation for the drag coefficient (C_d)

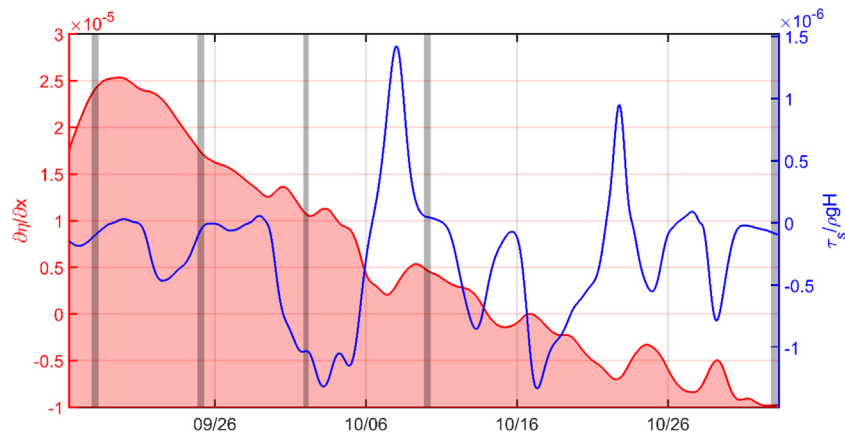


Fig. 10. Subtidal surface slope (red) between Wilcox and the estuary's mouth vs surface stress (blue). Dates of tidal-cycle experiments in gray vertical bands. (For interpretation of the references to color in this figure legend, the reader is referred to the web version of this article.)

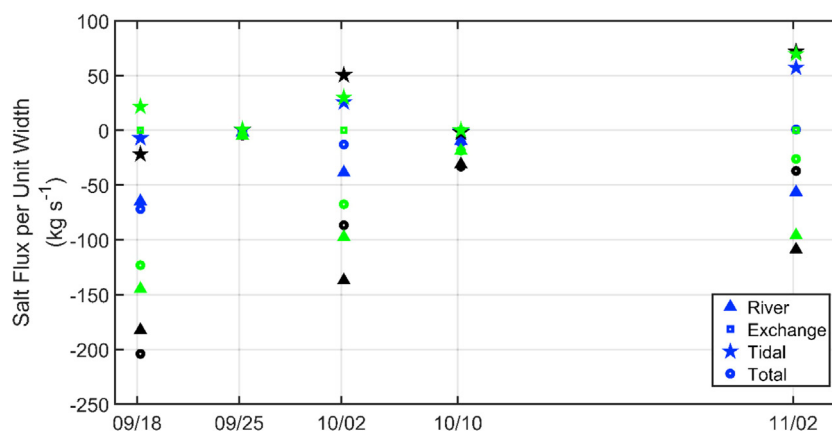


Fig. 11. Salt flux mechanisms for the along-estuary component at each transect and tidal-cycle experiment. Color coding: T1 in blue color, T2 in black color and T3 in green color. Symbol coding: Total salt flux (circle), river (triangle), exchange flow (square) and tidal pumping (star). (For interpretation of the references to color in this figure legend, the reader is referred to the web version of this article.)

from [Large and Pond \(1981\)](#), for a wind speed smaller than 10 m/s the drag coefficient (C_d) is estimated as a constant value of 0.00114 ([Large and Pond, 1981](#)). A valid approximation for the Suwannee River estuary where the maximum low-pass filtered winds were ~ 6 m/s.

Once the freshwater pulse started to recede and the along-estuary slope (between Wilcox and the mouth) decreased, the wind stress modified the water levels at the mouth of the estuary. Saltwater intrusion was enhanced due to wind stress acting on the water level. It was impossible to calculate bottom stress directly from measurements (no time series of velocities), so it was assumed that the imbalance between $\frac{\partial\eta}{\partial x}$ and $\frac{\tau_s}{g\rho H}$ ([Fig. 9](#)) is explained by bottom stresses. It is also possible that baroclinic effects could have played a role, but we have no information to verify these possibilities.

Saltwater pulses at the entrance to the estuary, over the shoals, occurred when the subtidal slope was $\partial\eta/\partial x < 1 \times 10^{-5}$ while wind direction changed within one day, i.e., on October 6th–7th, wind changed from SW to N. In addition, saltwater intrusion developed on Oct 02 and Nov 02 during flood tidal phases ([Fig. 3](#)). Again, the salt-wedge behavior in the estuary resulted in increased stratification during flood, contrary to what happens in other estuaries ([Simpson et al., 1990](#); [Friedrichs and Aubrey, 1988](#)). This is likely the result of tidal pumping of salt being the dominant mechanism, over mean and exchange flow for saltwater transport (e.g. [MacCready, 1999](#)), as explored below and with Eq. (4). Moreover, the vertically stratified water column

coincided with $\partial\eta/\partial x < 1 \times 10^{-5}$. After $\partial\eta/\partial x$ became $< 1 \times 10^{-5}$, wind forcing began to play a major role in saltwater intrusion ([Fig. 10](#)). Salinity increases at the mouth closely followed northward low-pass filtered winds ([Fig. 2](#)). Similar behavior was reported in the Atchafalaya Bay, where intrusions of saltwater ~ 2 g/kg occurred prior to the passage of cold fronts ([Li et al., 2011](#)). Intrusions of saltwater in Atchafalaya Bay lasted between 0.5 and 2 h, while in the Suwannee River estuary they lasted for the duration of the wind event. Numerical simulations in the Yangtze Estuary by [Li et al. \(2012\)](#) indicated that saltwater intrusion was also influenced by wind velocity.

Even though residual flows were seaward during the five tidal-cycle experiments, saltwater intruded in the deepest part of a cross-section during the flooding phase of the tide in three of the experiments. This suggested that tidal pumping ([Geyer and Nepf, 1996](#)) dominated salt fluxes rather than exchange flows, which usually dominate salt fluxes in partially stratified estuaries ([Monismith et al., 2002](#); [Bowen and Geyer, 2003](#); [Lerczak et al., 2006](#); [Ralston et al., 2008](#)). As part of the exchange flow, the down-gradient salt flux results from the spatial variations of salinity and currents, and from mixing at subtidal scales ([Taylor, 1953](#)). Tidal pumping is mainly related to the covariance of the tidal currents and salinity field ([Fischer, 1972](#); [Simpson et al., 2001](#)).

Fluxes from exchange flow and tidal pumping are estimated next for each of the five tidal-cycle experiments. The total salt flux (\mathcal{F}_s) considers, in addition to exchange flow and tidal pumping,

the seaward (or mean) transport of salt due to the river discharge (Lerczak et al., 2006):

$$\mathcal{F}_s = \left\langle \int_{-H}^0 (u_o S_o + u_E S_E + u_T S_T) dz \right\rangle = Q_f S_o + \mathcal{F}_E + \mathcal{F}_T \quad (4)$$

where \mathcal{F}_s is calculated here per unit of estuary's width because of the availability of only one profile of salinity across the transect. The salinity and velocities vary at subtidal scales ($u_o S_o$, $u_E S_E$) and tidal scales ($u_T S_T$). Velocities and salinities are decomposed in: tidally and cross-sectionally averaged ($u_o S_o$), tidally averaged and vertically varying ($u_E S_E$) and tidally and vertically varying ($u_T S_T$). The angle brackets indicate subtidal variations and the integral is in the vertical. The first term ($Q_f S_o$) is the advective transport of salt out of the estuary by the river discharge per unit of estuary's width Q_f ; the second term (\mathcal{F}_E) is the salt flux from the exchange flow or gravitational circulation (u_E) and the third term (\mathcal{F}_T) is the tidal oscillatory flux. Hereafter, the third term will be referred to as tidal pumping.

Each term of Eq. (4) was estimated for the three transects sampled during the tidal-cycle experiments (Fig. 11). Estimates of salt flux considered the velocity and salinity profiles recorded throughout the deepest profile of each transect. Positive values indicate saltwater intrusion or pulses of saltwater into the estuary and negative values indicate salt water directed out of the estuary. Minimum intrusion of saltwater occurred in the tidal-cycle experiments of Sept 25 and Oct 10 consistent with the values recorded with moored CT in the shallow portion of the estuary (Fig. 9). Maximum intrusions of saltwater occurred in the last tidal-cycle experiment of Nov 02 when the pulse of freshwater relaxed. Tidal pumping (colored stars) was the dominant mechanism driving saltwater into the estuary during the tidal-cycle experiments of Sept 18, Oct 02 and Nov 02, confirming the proposition advanced above. Slightly more intrusion of saltwater was observed in T2 (black stars) because its depth (~6 m) was greater than that at T1 and T3 (~3–4 m). Almost zero intrusion of saltwater occurred on Sept 25, just after the peak of the freshwater pulse (Fig. 11).

In general, the salinity field can respond in two ways during a freshwater pulse. Saltwater intrusion can be suppressed due to seaward advection of the salinity field by the river flow, or can be enhanced by strengthened exchange flows (Gong and Shen, 2011; Ralston et al., 2008; Valle-Levinson, 2012). Saltwater intrusion was suppressed in Alligator Pass after a moderate freshwater pulse (~500 m³/s) from Hurricane Irma. Salt water entered the estuary, however, via tidal pumping under minimum and negative water-level slopes.

6. Conclusions

This study at the Suwannee River estuary after the passage of Hurricane Irma, has yielded two main conclusions. First, the main mechanism responsible for driving salt water into Alligator Pass was tidal pumping, as expected for a salt-wedge estuary like the Suwannee River. This is contrary to what is expected in partially stratified estuaries, where salt fluxes are primarily associated with exchange flows. Second, the water-level slope inside the estuary modulated the intrusion of saltwater. Largest positive water-level slope inside the estuary occurred at the peak of the hurricane-related freshwater pulse. This positive slope caused seaward flows in the cross-section and limited the intrusion of saltwater. After the freshwater pulse relaxed, and the water-level slope inside the estuary was minimum or reversed to negative, the intrusion of saltwater was intensified by wind forcing. Largest excursions of saltwater occurred when the wind was blowing into the estuary, toward the north. It is expected that for a salt-wedge estuary like the Suwannee River estuary, the intrusion

of saltwater will be largest during spring tides and northward winds. In order to confirm this hypothesis, a longer measurement campaign would be required to cover at least two or more spring tidal cycles.

CRedit authorship contribution statement

Gisselle E. Guerra-Chanis: Writing - original draft, Investigation. **Sangdon So:** Investigation, Data collection, Resources, Review. **Arnoldo Valle-Levinson:** Supervision, Writing - review & editing, Funding acquisition.

Declaration of competing interest

The authors declare that they have no known competing financial interests or personal relationships that could have appeared to influence the work reported in this paper.

Acknowledgments

We are indebted to Braulio Juárez, Mohammad Al-Khaldi, Ahmad Yousif and Anne West-Valle for their helpful assistance in the field surveys. Two anonymous reviewers contributed substantially to the final manuscript. The study was supported by the Institute of International Education through their Global Innovation Initiative. GEGC thanks the support from Secretaría Nacional de Ciencia y Tecnología (SENACYT) from Panamá for her PhD studies. AVL acknowledges support from the NSF Project 1332718.

References

- Bowen, M.M., Geyer, W.R., 2003. Salt transport and the time-dependent salt balance of a partially stratified estuary. *J. Geophys. Res.* 108.
- Cangialosi, J.P., Latto, A.S., Berg, R., 2017. National Hurricane Center Tropical Cyclone Report Hurricane Irma. NOAAAL112017.
- Cho, K.-H., Wang, H.V., Shen, J., Valle-Levinson, A., Teng, Y.-c., 2012. A modeling study on the response of Chesapeake Bay to hurricane events of Floyd and Isabel. *Ocean Model.* 49–50, 22–46.
- Fischer, H., 1972. Mass transport mechanisms in partially stratified estuaries. *J. Fluid Mech.* 53 (4), 671–687.
- Friedrichs, C.T., Aubrey, D.G., 1988. Non-linear tidal distortion in shallow well-mixed estuaries: a synthesis. *Estuar. Coast. Shelf Sci.* 27 (5), 521–545.
- Garvine, R.W., 1991. Subtidal frequency estuary-shelf interaction: Observations near Delaware Bay. *J. Geophys. Res.: Oceans* 96 (C4), 7049–7064.
- Geyer, W.R., MacCready, P., 2014. The Estuarine Circulation. *Annu. Rev. Fluid Mech.* 46 (1), 175–197.
- Geyer, W.R., Nepf, H., 1996. Tidal Pumping of Salt in a Moderately Stratified Estuary. *Buoyancy Effects on Coastal and Estuarine Dynamics*.
- Gong, W., Shen, J., 2011. The response of salt intrusion to changes in river discharge and tidal mixing during the dry season in the Modaomen Estuary, China.. *Cont. Shelf Res.* (31), 769–788.
- Henrie, K., Valle-Levinson, A., 2014. Subtidal variability in water levels inside a subtropical estuary. *J. Geophys. Res.: Oceans* 119 (11), 7483–7492.
- Joyce, T.M., 1989. On in Situ Calibration of Shipboard ADCPs. *J. Atmos. Ocean. Technol.* 6 (1), 169–172.
- Large, W.G., Pond, S., 1981. Open ocean momentum flux measurements in Moderate to Strong Winds. *J. Phys. Oceanogr.* 11 (3), 324–336.
- Laurel-Castillo, J.A., Valle-Levinson, A., 2020. Tidal and subtidal variations in water level produced by Ocean-River interactions in a Subtropical Estuary. *J. Geophys. Res.: Oceans* 125 (7), e2018JC014116.
- Lerczak, J.A., Geyer, W.R., Chant, R.J., 2006. Mechanisms driving the time-dependent Salt Flux in a Partially Stratified Estuary. *J. Phys. Oceanogr.* 36 (12), 2296–2311.
- Li, C., Roberts, H., Stone, G.W., Weeks, E., Luo, Y., 2011. Wind surge and saltwater intrusion in atchafalaya bay during onshore winds prior to cold front passage. *Hydrobiologia* 658 (1), 27–39.
- Li, L., Zhu, J., Wu, H., 2012. Impacts of wind stress on saltwater intrusion in the Yangtze Estuary. *Sci. China Earth Sci.* 55 (7), 1178–1192.
- Light, H.M., Darst, M.R., Lewis, L.J., Howell, D.A., 2002. Hydrology, vegetation, and soils of riverine and tidal floodplain forests of the lower Suwannee River, Florida, and potential impacts of flow reductions. In: U.S. Geological Survey Professional Paper 1656-A. p. 124.
- MacCready, P., 1999. Estuarine adjustment to changes in River Flow and Tidal mixing. *J. Phys. Oceanogr.* 29, 708–726.

- MacCready, P., 2007. Estuarine adjustment. *J. Phys. Oceanogr.* 213, 3–2145.
- McDougall, T.J., Barker, P.M., 2011. Getting started with TEOS-10 and the Gibbs Seawater (GSW) Oceanographic Toolbox. In: SCOR/IAPSO WG 127. p. 28.
- McDougall, T.C., Jackett, D.R., Millero, F.J., Pawlowicz, R., Barker, P.M., 2012. A global algorithm for estimating Absolute Salinity. *Ocean Sci.* (8), 1123–1134.
- Monismith, S.G., Kimmerer, W., Burau, J.R., Stacey, M.T., 2002. Structure and flow-induced variability of the subtidal Salinity field in Northern San Francisco Bay. *J. Phys. Oceanogr.* (32), 3003–3019.
- Muste, M., Yu, K., Spasojevic, M., 2004. Practical aspects of ADCP data use for quantification of mean river flow characteristics; Part I: moving-vessel measurements. *Flow Meas. Instrum.* 15 (1), 1–16.
- Payandeh, A.R., Justic, D., Mariotti, G., Huang, H., Sorourian, S., 2019. Subtidal water level and current variability in a Bar-built estuary during Cold Front Season: Barataria Bay, Gulf of Mexico. *J. Geophys. Res.: Oceans* 124 (10), 7226–7246.
- Pollard, R., Read, J., 1989. A method for calibrating Shipmounted Acoustic Doppler Profilers and the limitations of Gyro Compasses. *J. Atmos. Ocean. Technol.* 6 (6), 859–865.
- Ralston, D.K., Geyer, W.R., Lerczak, J.A., 2008. Subtidal salinity and velocity in the Hudson River Estuary: Observations and Modeling. *J. Phys. Oceanogr.* 38 (4), 753–770.
- Salas-Monreal, D., Valle-Levinson, A., 2008. Sea-level slopes and volume fluxes produced by atmospheric forcing in estuaries: Chesapeake Bay case study. *J. Coast. Res.* (24), 208–217.
- Scully, M.E., Friedrichs, C., Brubaker, J., 2005. Control of estuarine stratification and mixing by wind-induced straining of the estuarine density field. *Estuaries* 28 (3), 321–326.
- Scully, M.E., Geyer, W.R., Lerczak, J.A., 2009. The influence of lateral advection on the Residual Estuarine circulation: A numerical Modeling Study of the Hudson River Estuary. *J. Phys. Oceanogr.* 39 (1), 107–124.
- Simpson, J.H., Brown, J., Matthews, J., Allen, G., 1990. Tidal straining, density currents, and stirring in the control of estuarine stratification. *Estuaries* 13 (2), 125–132.
- Simpson, J.H., Vennell, R., Souza, A.J., 2001. The salt fluxes in a Tidally-Energetic Estuary. *Estuar. Coast. Shelf Sci.* (52), 131–142.
- Smith, J.A., Villarini, G., Baeck, M.L., 2010. Mixture distributions and the Hydroclimatology of Extreme Rainfall and Flooding in the Eastern United States. *J. Hydrometeorol.* 12 (2), 294–309.
- So, S., Juarez, B., Valle-Levinson, A., Gillin, M.E., 2019. Storm surge from Hurricane Irma along the Florida Peninsula. *Estuar. Coast. Shelf Sci.* 229, 106402.
- So, S., Valle-Levinson, A., Laurel-Castillo, J.A., Ahn, J., Al-Khalidi, M., 2020. Removing wave bias from velocity measurements for Tracer Transport: The Harmonic Analysis approach. *Water* 12 (4).
- Taylor, G.T., 1953. Dispersion of soluble matter in solvent flowing slowly through a tube. *Proc. R. Soc. A* 219 (1137), 186.
- Tillis, G.M., 1999. Flow and Salinity Characteristics of the Upper Suwannee River Estuary, Florida. USGS.
- Valle-Levinson, A., 2012. Impact of record flooding of a subtropical river on estuary/ocean exchange. *Ocean Dyn.* 62, 77–85.
- Valle-Levinson, A., Huguenard, K., Ross, L., Branyon, J., MacMahan, J., Reniers, A., 2015. Tidal and nontidal exchange at a subtropical inlet: Destin Inlet, Northwest Florida. *Estuar. Coast. Shelf Sci.* 155, 137–147.
- Valle-Levinson, Arnoldo, Lwiza, Kamazima, 1997. Bathymetric influences on the lower Chesapeake Bay hydrography. *J. Mar. Syst.* 12, 221–236.
- Valle-Levinson, A., Wong, K.-C., Bosley, K.T., 2002. Response of the lower Chesapeake Bay to forcing from Hurricane Floyd. *Cont. Shelf Res.* 22 (11), 1715–1729.
- Villarini, G., Smith, J.A., Baeck, M.L., Marchok, T., Vecchi, G.A., 2011. Characterization of rainfall distribution and flooding associated with U.S. landfalling tropical cyclones: Analyses of hurricanes Frances, Ivan, and Jeanne 2004. *J. Geophys. Res.: Atmos.* 116 (D23).
- Warner, J.C., Geyer, W.R., Lerczak, J.A., 2005. Numerical modeling of an estuary: A comprehensive skill assessment. *J. Geophys. Res.*
- Wen-Cheng, L., Ming-Hsi, H., Kuo, A.Y., Jan-Tai, K., 2001. The influence of river discharge on Salinity intrusion in the Tanshui Estuary, Taiwan. *J. Coast. Res.* 17 (3), 544–552.
- Wu, H., Zhu, J., Ho Choi, B., 2010. Links between saltwater intrusion and subtidal circulation in the Changjiang Estuary: A model-guided study. *Cont. Shelf Res.* 30 (17), 1891–1905.